Crystal and Electronic Study of Neodymium-Substituted $CuFeO_2$ Oxide

OSMAN MURAT OZKENDIR

Neodymium-substituted $CuFeO_2$ samples were investigated according to their crystal and electronic properties *via* the general formula $Nd_xCu_{1-x}FeO_2$. The crystal structure analysis results revealed polycrystalline formations in the sample and a change in crystalline sizes with the substituted heavy fermion "Nd." Increasing the Nd amount in the sample was determined to cause a disturbance on the Cu-Fe planes that supports the formation of crystal structures with low crystal symmetries such as monoclinic or triclinic geometries. To obtain the background mechanisms of the crystal properties, the X-ray absorption fine structure spectroscopy technique was used to study the electronic properties of the samples. Prominent changes in the crystal structures due to 4*f* electrons' contributions from the substituted Nd atoms as the main "role player" in the phase transitions were determined. The Nd atoms were observed as the key element guiding the entire phenomenon as a result of their large size and narrow 4*f* levels. Also, magnetic properties of the samples were tested at room temperature and without an applied magnetic field by X-ray magnetic circular dichroism study due to previous studies that reported the parent oxide $CuFeO_2$ to have magnetic ordering at $T_N = 11$ K (−262 °C). Except the sample for $x = 1.0$ ($NdFeO_3$), no magnetic ordering was observed at room temperature; *i.e.*, all of the samples showed paramagnetic behaviors.

DOI: 10.1007/s11661-016-3457-z

I. INTRODUCTION

IRON oxides are a popular class of transition metal oxides (TMOs) studied with a broad range of research subjects such as batteries, magnetic materials, semiconductors, minerals, electronics, and optoelectronic devices.[1–5] The *d* shells of the TMs are also a playground for strong electronic correlations with the outer shell electrons of the neighboring atoms. Strongly correlated electron systems are a large class of compounds with elements that have unoccupied *d*- or *f*-electron shells with narrow energy bands. Due to the narrow energy bands (with high quantum symmetry), the *d*-*f* system interactions attract considerable attention in scientific studies because of the possibility of yielding fruitful results for technological applications. Additionally, a large amount of studies reported that several TMOs have dominant nonspatially homogeneous states occuring when several physical interactions such as charge, spin, lattice, or orbital are active simultaneously.[6]

$CuFeO_2$ is an important member of iron oxides as a low-dimensional TMOs with delafossite rhombohedral *R-3m* crystal geometry.[2–4] The popularity of the $CuFeO_2$ oxides comes from their geometrically frustrated antiferromagnetic (AFM) [$T_N = 11$ K (−262 °C)] character. Delafossite $CuFeO_2$ oxide crystal structure forms in slightly distorted triangular geometry with hexagonal layers. However, the crystal structure is highly affected by oxygen nonstoichiometry related with the change in cation valence bands.[2] Mainly, the bonding mechanism in the $CuFeO_2$ oxide is governed by its 3*d* row elements Fe and Cu. When the 3*d* levels are presented in an environment where atoms get close to each other, they are the main role players during interatomic interactions with fivefold degeneracy. Partly occupied *d* shells of the TMs are the source of rich quantum symmetry in electronic interactions and reveal interesting physical phenomena exhibiting desired crystallographic, magnetic, electronic, or chemical properties.[4–9]

In this study, the influence of the heavy fermion "Nd" substitution into the delafossite $CuFeO_2$ structures was investigated in the crystal and electronic properties of the samples *via* the general formula $Nd_xCu_{1-x}FeO_2$. The study was inspired by the interesting properties of the $CuFeO_2$ that were reported in several previous studies, such as its possesing rich various magnetic phases at low temperature and paramagnetic behaviors at room temperature due to frusturated crystal structures, ferroelectricity, and vibratrional anisotropy.[10] Here, the author's main goal is to investigate the electronic and crystal structure background of the delafossite CuFeO2 material and its amazing properties by substituting a rare earth element where highly active *f*-electrons are the main players in the molecular interplays.

$Nd_xCu_{1-x}FeO_2$ samples, where *x* has a value of 0.0, 0.2, 0.4, 0.8, or 1, were prepared by the classical solid-state reaction method. Samples were prepared in

OSMAN MURAT OZKENDIR, Associate Professor, is with the Energy Systems Engineering, Tarsus Faculty of Technology, Mersin University, Tarsus, Turkey. Contact email: ozkendir@gmail.com
Manuscript submitted December 11, 2015.
Article published online March 31, 2016

powder form. The samples were synthesized from the stoichiometric mixtures of Nd_2O_3, Cu_2O, and α-Fe_2O_3 powder compounds as starting materials with high purity (Alfa-Aesar (Germany), metal basis >99 pct). The solid-state reaction method is one of the most popular methods for the preparation of bulk and powder materials by mixing parent materials. To obtain the best results to achieve the desired materials, the mixed materials should be milled and annealed until the desired reactions take place. So the samples were milled in ethanol by a magnetic stirrer at room temperature for 12 hours. In the second step, the samples were annealed up to 523 K (250 °C) for 6 hours and dried in air. Then the samples were remilled in ethanol at room temperature for 24 hours and dried in air.

Prior to the study, the magnetic behaviors of all prepared samples were tested at room temperature by physical property measurement system (PPMS) measurements. The results of the measurements highlighted interesting electronic interactions yielding unfamiliar magnetic properties *via f*-electrons' contribution. Magnetic ordering at room temperature was determined as $CuFeO_2$ ($x = 0$), $NdFeO_3$ ($x = 1$), and $Nd_{0.4}Cu_{0.6}FeO_2$ samples showing paramagnetic ordering; however, samples $Nd_{0.2}Cu_{0.8}FeO_2$ and $Nd_{0.8}Cu_{0.2}FeO_2$ showed weak AFM ordering.

II. MATERIALS AND METHODS

To study the crystal structure properties of the Nd-doped $CuFeO_2$ samples, and also to determine the background information for further extended-X-ray absorption fine structure spectroscopy (EXAFS) analysis, X-ray diffraction (XRD) patterns of the samples were taken at the Advanced Materials Research Laboratory, Mersin University (Mersin, Turkey), with the Rigaku (Japan) Smartlab model. In Figure 1, XRD patterns of the samples are given in comparison with all doped and undoped samples. According to Figure 1, all samples present multiplet diffraction patterns highlighting the polycrystalline nature of the samples. The sample for $x = 1.0$ ($NdFeO_3$) has a smooth pattern among all sample patterns and points out one crystal geometry formation in the bulk (Table I). The samples for $x = 0.2$ and 0.4 have more peak features with noiselike weak edges reflecting the polycrystalline structure with a different or weak crystal symmetry. As a guide for sample patterns, reflections of the intensities were defined and given in the figure for the $CuFeO_2$ sample. The reflection of the highest peak intensity on the pattern was determined from the [110] plane and confirms the highest crystal formations as $CuFeO_2$ in the bulk. Besides, reflections for hematite (α-Fe_2O_3) structure were also determined as the secondary formation in the polycrystalline sample for $x = 0.0$. With increasing Nd substitutions, Nd reflections increase and become more intense, while Cu-centered reflections have a meaningful decay. Also, some asymmetric change with the substitution ratio at Nd sites is a result of the change in site symmetries due to crystal geometries of the elements.

The noisy patterns of the low Nd samples indicate the influence of a heavy atom existence on the crystal morphology of the samples. The change in the morphology can be best observed by the average crystallite sizes in the crystals. For this purpose, the average crystallite sizes of the substituted samples were estimated with the XRD patterns taken *via* the Scherrer formula,[11] given as

$$A = K\lambda/(\beta \cos\theta) \quad [1]$$

Here, A is the average crystallite size, λ is the wavelength of the X-ray beam used (0.154056 nm), K is the Scherrer constant (0.94),[12,13] θ is the Bragg angle, and β is the full-width at half-maximum (FWHM) of the diffraction. The calculated average crystallite sizes for $Nd_xCu_{1-x}FeO_2$-substituted materials are given in Figure 2. The crystallite sizes of the samples were determined to vary between 44 and 63 nm, as given in the figure, and experienced a meaningful increase with the Nd substitution amount. Heavy Nd atoms built larger crystal complexes and increased the grain size with possible porosity in the samples.

To reveal the background information of the crystal structure of the samples, collected XRD patterns were used in the analysis performed by the material analysis using diffraction (MAUD) software. The MAUD software works for XRD patterns and is the research result of Luca Lutterotti from Italy. It is a diffraction/reflectivity analysis code, mainly based on the Rietveld method.[14] The results of the XRD pattern analysis for all samples are given in Table I. According to the analysis, the sample for $x = 0.0$ formed in the polycrystalline structure and mainly formed in the $CuFeO_2$ structure (80 pct), which was aimed to be prepared. The crystal geometry of $CuFeO_2$ is determined as trigonal with a space group of *R-3m:R*. The lattice parameters are estimated as $a = 5.237$ Å and $\alpha = \beta = \gamma = 33.54$ deg. Twenty percent in the sample was determined as the parent α-Fe_2O_3 crystal structure with trigonal but had a different space group of *R-3m:R* than did the parent oxide.

The sample for $x = 0.2$ had a noisy XRD pattern and analysis revealed three different crystal structure formations in the bulk, which were highly responsible from the noisy pattern. Only 15 pct of the sample remained in the $CuFeO_2$ crystal structure. The main crystal structure in this sample was determined as $CuFe_2O_4$ (56 pct) with tetragonal geometry and space group of *I41/amd:2*. The rest of the bulk sample (29 pct) was determined as formed in the $Nd_6Cu_3Fe_4O_{24}$ structure with triclinic geometry and had *P-1* space group. Poor site symmetry of the triclinic crystal formation seemed to be the secondary reason for the noisy crystal structure. It played the role of defect formation in the sample.

The sample for $x = 0.4$ has the noisiest XRD pattern. However, crystal structure analysis revealed only one type of geometry and structure formation in the entire bulk: monoclinic $Nd_4Cu_2Fe_2O_{13}$ crystal with *P21/m:b* space group. The low symmetry of the geometry caused a high noisy pattern and possibly promoted the effects of the defects in the bulk. Because, despite the advantage of only one geometry formation in the bulk, it had a noisier

pattern than the sample for $x = 0.2$. In such case, one should always keep in mind the fact that low symmetry in a crystal may have disadvantages for some optical properties, but it may be a blessing in other aspects such as electrical, electronic, or magnetic properties.

Unlike the noisy pattern of the samples for $x = 0.2$ and 0.4, the XRD pattern of the sample for $x = 0.8$ was smoother. The less noisy structure is obviously related to the number of different crystal structure formations and the symmetry of the crystal geometries. The sample for $x = 0.8$ formed with two different crystal structures: 37 pct in trigonal $CuFeO_2$ (*R-3m*:*R*) and 63 pct in monoclinic $Nd_4Cu_2Fe_2O_{13}$ crystal with *P21*/*m*:*b* space group such as the sample for $x = 0.4$. The monoclinic crystal structure $Nd_4Cu_2Fe_2O_{13}$ seemed the most preferable geometry of the Nd-Cu-Fe-O complexes.

The sample for $x = 1.0$ has the smoothest XRD pattern among all samples. The sample was determined as being formed in the $NdFeO_3$ crystal structure with orthorhombic geometry and *Pnma* space group. The hematite reflections on the XRD pattern of the sample $x = 1.0$ showed great decay but did not disappear at all. The blurry hematite reflections highlighted a heavy fermion Nd link to hematite-like ligands to form the $NdFeO_3$ crystals. To illuminate the physics beneath such crystal behaviors, traces of the bonding interactions between atoms resulting in the reported crystal structure formations should be probed; the XAFS technique was one of the best candidates for this study.

XAFS is one of the most popular techniques that uses synchrotron light in electronic and crystal structure investigations. For the XAFS study, collected data can be processed in two parts: by X-ray absorption near-edge spectroscopy (XANES) and EXAFS. While the EXAFS data can yield fruitful information to support the crystal structure study, XANES can provide information about bonding with the neighboring atoms and the electronic structure of the interested atoms in the materials as well as support the determination of local atomic arrangements in the materials.

For the electronic structure study, XANES data were collected at the I1011 beamline of the MAX-Lab Synchrotron Laboratory, which is located in the Lund University campus area in Lund, Sweden. The beamline I1011 delivers light from the ring MAX-II that uses an elliptically polarizing undulator and provides soft X-ray with a variable polarization state.[15] Fe $L_{3,2}$-edge and O K-edge measurements were performed at ultra high vacuum (UHV) conditions ($\sim 10^{-10}$ Torr) and at room-temperature conditions. The collected spectra were recorded with a total electron yield mode by detecting a drain current from the sample, and the energy resolution was set to 0.1 eV.

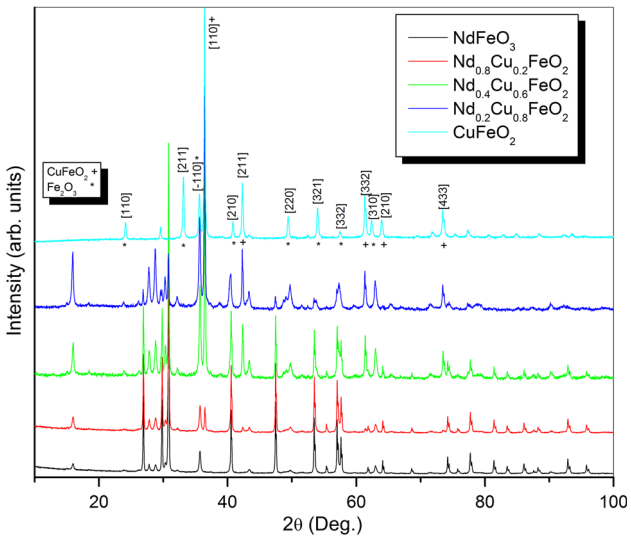

Fig. 1—Comparison of the XRD patterns of the $Nd_xCu_{1-x}FeO_{2+d}$ samples.

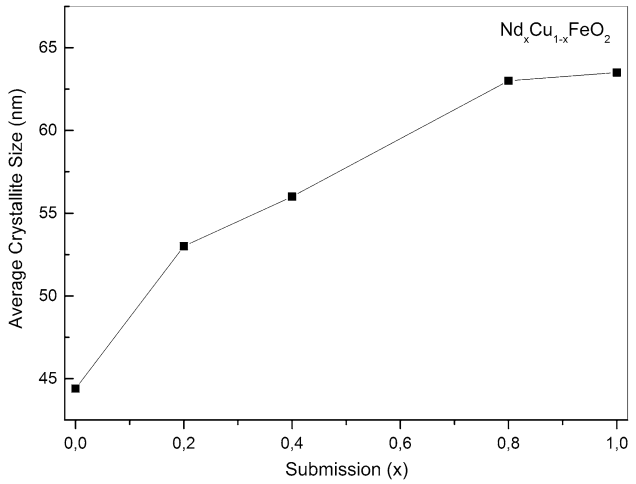

Fig. 2—Average crystallite sizes of the $Nd_xCu_{1-x}FeO_{2+d}$ samples.

Table I. XRD Pattern Results of Nd-Doped $CuFeO_2$ Samples

Substitution ($Nd_xCu_{1-x}FeO_2$)	Crystal	α	β	γ	*a*	*b*	*c*	Geometry	SG	Pct
$x = 0$	$CuFeO_2$	33.54	33.54	33.54	5.237	5.237	5.237	trigonal	*R*-3*m*:*R*	80
	Fe_2O_3	55.23	55.23	55.23	5.441	5.441	5.441	trigonal	*R*-3*m*:*R*	20
$x = 0.2$	$CuFe_2O_4$	90	90	90	5.770	5.770	8.561	tetragonal	*I*41/*amd*:2	56
	$CuFeO_2$	29.93	29.93	29.93	5.901	5.901	5.901	trigonal	*R*-3*m*:*R*	15
	$Nd_6Cu_3Fe_4O_{24}$	107.78	100.88	103.32	7.641	9.261	6.260	triclinic	*P*-1	29
$x = 0.4$	$Nd_4Cu_2Fe_2O_{13}$	90	95.53	90	12.633	8.282	5.410	monoclinic	*P*21/*m*:*b*	100
$x = 0.8$	$CuFeO_2$	30.59	30.59	30.59	5.757	5.757	5.757	trigonal	R-3*m*:*R*	37
	$Nd_4Cu_2Fe_2O_{13}$	90	95.69	90	12.035	8.483	4.830	monoclinic	P21/*m*:*b*	63
$x = 1.0$	$NdFeO_3$	90	90	90	6.783	8.562	5.249	orthorhombic	*Pnma*	100

The Fe $L_{3,2}$-edge XANES spectra of parent $CuFeO_2$ is given in Figure 3. The shape of the spectra in the figure compels us to analyze the absorption edges in three parts: pre-edge, main-edge and post-edge. The L-edge spectra is a result of strong spin-orbit interaction between $2p$ core holes with $3d$ final states, and the crystal field splits the energies of the states into two levels that are given as separate L_3 and L_2 peaks. The L_3-edge absorption peak is due to the transition of the $2p_{3/2}$ core electrons to the unoccupied $3d$ levels, while the L_2 edge absorption peak corresponds to the transition of the $2p_{1/2}$ core electrons to the empty $3d$ final states.[2,4]

In the figure, the Fe L_3-edge absorption spectra of the sample with 80 pct $CuFeO_2$ and 20 pct α-Fe_2O_3 begin to rise at 703 eV and have two maxima with a weak edge at 705.5 eV and the main edge at 707.1 eV. The two-peak feature of the L_3-edge spectra highlights the occurrence of two different site symmetries in the sample. The geometries of the crystal formations in the sample are the same (trigonal) but have different angle degrees. Besides, the ratio of the FWHM values of the peaks is estimated as 3.97, and the result confirms 80 pct $CuFeO_2$ (highest peak) and 20 pct α-Fe_2O_3 (lower peak) crystal formations in the bulk, as given in Table I. The intensities of the peaks on the spectra are related to the unoccupied states at the valence level of the Fe^{3+} ion (*i.e.*, $[Ar]4s^0 3d^5$), where excited electrons can find a place as a final state. Beyond the main edge, a weak edge at 710.2 eV appears, like a bump, addressing the *d-d* metal bonding between the Cu-Fe atoms at the higher energy levels of the molecular band. It can be summarized here that the fivefold degeneracy of the iron atoms provides low-energy t_{2g} (xy, yz, xz) for the pre-edge and main-edge levels. However, weakly interacting metals bond through the high-energy e_g ($x^2 - y^2$, $3z^2 - r^2$) levels. Oxygen atoms can surround the metal atoms, and they can easily overlap by interacting with the outer shell electrons of the metal atoms (Cu, Fe). When atoms get closer (so the outer shells), and if they have convenient quantum symmetries with close energies, they can overlap strongly and build broad molecular bands. The sharp peaks of the Fe-L_3 absorption edge are relevant to its oxidation state and highlight the strongly overlapped Fe-O outer shell electrons. However, the weaker intensity beyond the main edge is due to poorly interacting Fe-Cu outer shell electrons, an indication of large molecular band formation. A similar two-peak feature of L_3-edge spectra is also presented at the L_2-edge spectra with maxima at 718.8 and 720.3 eV, respectively.

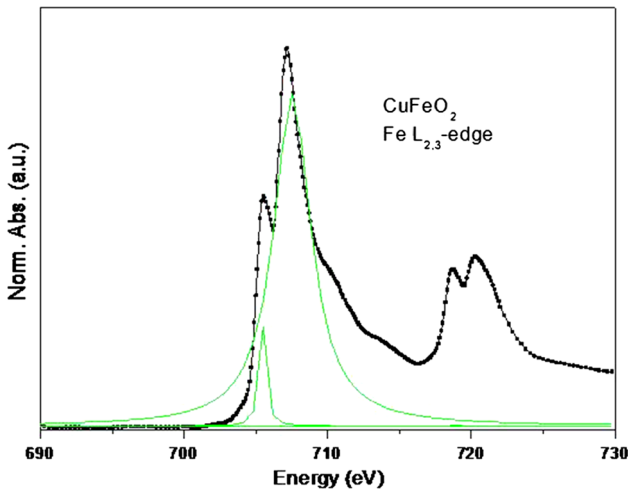

Fig. 3—Fe $L_{3,2}$ edge XANES spectra of the sample for $x = 0.0$.

In Figure 4, Fe $L_{3,2}$-edge spectra of $CuFeO_2$, $Nd_{0.4}Cu_{0.6}FeO_2$, and $NdFeO_3$ samples ($x = 0.0$, 0.4, and 1.0) are given in comparison. For the comparison, the $Nd_{0.4}Cu_{0.6}FeO_2$ sample is chosen because of its crystal structure, which has poor site symmetry but formed dominantly in the samples for $x = 0.4$ and 0.8. Besides, this structure is a good candidate for the study that can reflect the Nd influence on the electronic interactions. In the figure, according to the reference Fe $L_{3,2}$-edge spectra of the sample for $x = 0$ (*i.e.*, 80 pct $CuFeO_2$ + 20 pct Fe_2O_3), other Fe $L_{3,2}$-edge spectra have slight energy shifts to lower energy sides with 0.5 eV for $Nd_{0.4}Cu_{0.6}FeO_2$ and 0.9 eV for $NdFeO_3$ samples. The energy shifts to lower energy side point out the anionic characters of Fe atoms in the samples by gaining electrons mainly from oxygen atoms *via* bonding and also *4f* contribution to the molecular band by Nd substitution. On the Fe $L_{3,2}$-edge spectra, the higher energy shift of $NdFeO_3$ than $Nd_{0.4}Cu_{0.6}FeO_2$ also confirms the higher quantum symmetry gain *via p-d-f* hybridized molecular bands. The *f*-level support becomes clearer at the $NdFeO_3$ spectra with a weak pre-edge feature at 702.5 eV, which is assigned "A." The pre-edge features are caused by the electronic transitions that do not obey the quantum selection rules ($\Delta l = \pm 1$), which control the transition probability of the excited electrons by the dipolar selection rules or highlight the crystal structure disorders in the samples. The pre-edge part of the absorption spectra can provide us information about the dependence on the oxidation states of the neighbors, chemical shifts, or geometry around the absorbing atom.[16] The pre-edge feature on the spectra for the $x = 0.4$ sample is weaker than that on the $NdFeO_3$ sample. The intensity change in the pre-edge confirms the $4f$ contribution to the electronic state generation on the molecular band. The multiplet structure on the $4f$ level of the Nd atoms, as given in the inset of the figure for $M_{4,5}$-edge absorption spectra of the Nd^{3+} atoms, also supports the increase at the highest peak as a result of strong overlapping between Fe $3d$ and Nd $4f$ levels.

The peak below the L_3-edge of the sample $x = 0.0$ ($CuFeO_2$), assigned as B, has a meaningful decay for the sample $x = 0.4$ but has higher intensity at the spectra for the sample $x = 1.0$ ($NdFeO_3$). The change in the lower energy edge feature points out the rhombohedral symmetry existence on the Fe sites in all samples. This feature is also confirmed in XRD patterns with the weak but not disappearing hematite reflection intensities. Additionally, the L-edge spectra preserves its multiplet character in all samples and highlights strong overlapping between Fe and O atoms with $2p$-$3d$ hybridization.

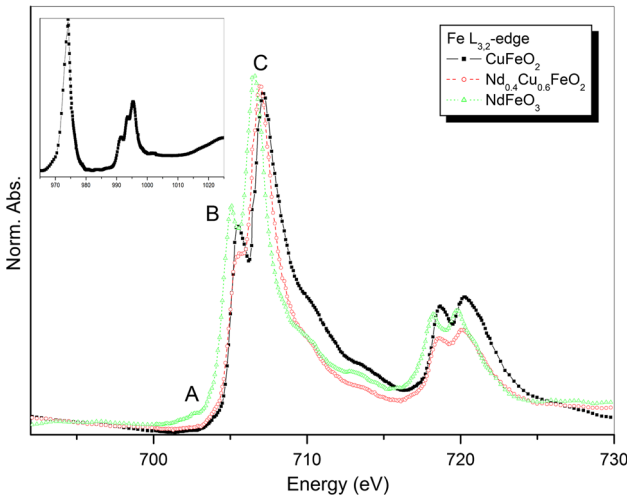

Fig. 4—Comparison of the Fe $L_{3,2}$-edge XANES spectra of the samples for $x = 0.0$, 0.4, and 1.0. Inset: Nd $M_{4,5}$-edge XANES spectra in $NdFeO_3$.

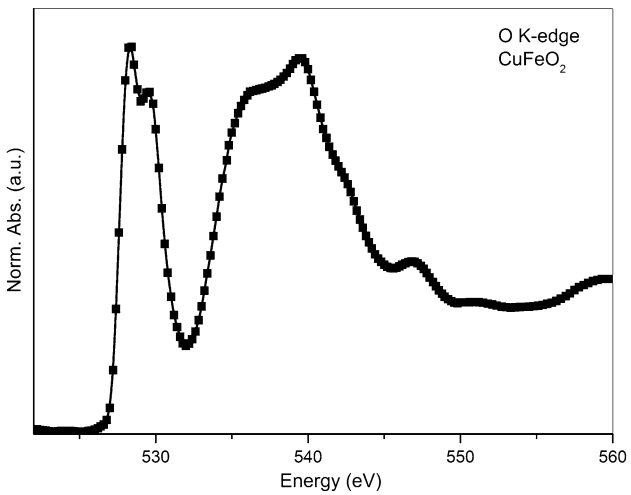

Fig. 5—Oxygen K-edge XANES spectra of the sample for $x = 0.0$.

To obtain a better view of the atomic interactions, O K-edge XANES spectral analysis can provide us better evidence on the bonding interactions of the $Nd_xCu_{1-x}FeO_2$ samples. For this aim, O K-edge XANES spectra of $CuFeO_2$ (for sample $x = 0$) are given as the reference tool in Figure 5 and the comparison of O K-edge absorption spectra of the samples are given in Figure 6. High electronegativity of the oxygen provides the ability to interact with almost all neighboring atoms *via* bonding. This ability keeps them in the center of all interactions and makes oxygen atoms an important tool for investigations. Thus, absorption edges of the oxygen atoms are sensitive to local bonding and symmetry.

In Figure 5, a splitted pre-edge feature with two sharp peaks is seen on the O K-edge spectra of the sample for $x = 0.0$. The splitted pre-edge structure is a result of different bond properties with iron because of the different angle degrees of the rhombohedral $CuFeO_2$ and α-Fe_2O_3 crystals. The pre-edge structure has the highest peak at 528.4 eV and a second peak with slightly

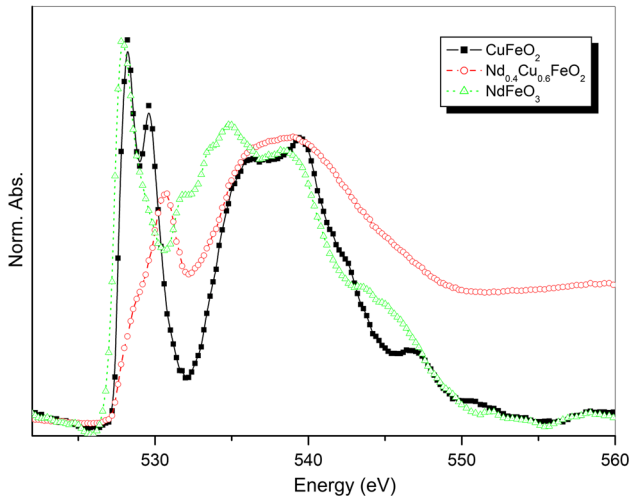

Fig. 6—Comparison of the oxygen K-edge XANES spectra of the samples for $x = 0.0$, 0.4, and 1.0.

lower intensity beyond it at 529.45 eV. The first peak is related to lower energy levels on the hybrid *p-d* molecular bands. Here, the pre-edge is due to electrons' forbidden transitions according to the dipole selection rules, because the excited *s* electrons' main route should be the *p* levels, not the *d* levels. However, hybridized *p*-like *d* levels of the iron atoms make the *d* levels available (weakly) as a final state. However, hybridization makes the molecular bands rich in quantum symmetry and lowers the band energies with the gained excess quantum symmetry *via d*-level interactions in the constructed broad molecular bands. The pre-edge feature also gives us clues about the crystal structure differences in the samples generated by electronic interactions. The main absorption peak of the O K-edge has broad structure with two maxima at 536.3 and 539.5 eV, respectively. The main absorption peak of the O K-edge corresponds to the transition of the excited 1*s* electrons of the oxygen atoms to unoccupied 2*p* levels as final states.

Comparison of the O K-edge absorption spectra of the samples for $x = 0.0$, 0.4, and 1.0 is given in Figure 6. $Nd_{0.4}Cu_{0.6}FeO_2$ ($x = 0.4$) and $NdFeO_3$ ($x = 1.0$) sample spectra have different pre-edge structures than the $CuFeO_2$ spectra. The main difference is the decay at the second pre-edge peak feature. There is only one sharp peak observed and it is almost joined with the main edge. For the $NdFeO_3$ sample, the highest pre-edge peak has a maximum at 528 eV and the spectra have a 1 eV shift to the lower energy side. The pre-edge part in sample $Nd_{0.4}Cu_{0.6}FeO_2$ almost changed and was observed as a lower energy part of the main edge. The absorption spectra highlights the monoclinic crystal symmetry with its multiplet structure. The main edge of the sample also has a 0.4-eV shift to the lower energy side and a large Gaussian shape with multiple bumplike weak structures. Large absorption edges of the samples for $x = 0.4$ and 1.0 also highlight the *f*-electron contribution to the molecular bands with a typical multiplet Nd spectral feature.

Crystal structure of the samples can also be probed by the photoelectron activities during the electron excitation with excess photon energy over the binding energy of the interested source atom. If the photoelectrons are excited with a kinetic energy, they can scatter from the neighboring atoms and their wave functions can interact with the incoming X-rays. Constructive or destructive interactions of the wavefunctions produce fluctuations on the absorption spectra from 80 to 100 eV beyond the XANES part to 800 to 1000 eV. This part of the spectra contains information about the local geometrical structures and is called the EXAFS spectra.[16–18]

The XAFS spectroscopy data were collected at the Beamline BL8:XAS of the Siam Photon (SLRI) Synchrotron Radiation facility in Nakhon Ratschasima, Thailand.[19,20]

The beamline operates for X-ray absorption spectroscopy (XAS) and serves a high flux light from a bending magnet with an energy range of 1.25 to 10 keV. Measurements were performed at room temperature in transmission mode for Cu K-edge. Also, in order to theoretically support the collected XAFS data, calculations were performed for Cu K-edge using the the real space multiple scattering approach FEFF 8.2 code.[16–18] The calculations were run with the input files generated by the TkATOMS code.[21] A copper atom in the input file was selected as the absorber and photoelectron emitter. The input file was generated for 15-Å thick $CuFeO_2$ cluster containing 467 atoms (Cu,Fe,O). In Figure 7, the Cu K-edge XAFS spectra of the Cu foil, which is the reference material in the study, are given in comparison with the $CuFeO_2$ measurement and calculation. The calculated spectra exhibit good agreement with the measured spectra. The Cu K-edge spectra of the Cu foil begin to rise at 8965 eV and have a maximum at 8997 eV as the main-edge peak. Strong fluctuations beyond the main edge of the Cu foil highlight the high-energy photoelectron activities, briefly scattering from the close neighboring (Cu) atoms that surround the source Cu atom. At 8956 eV, a weak pre-edge structure is observed as a result of *1s-3d* forbidden transition and highlighted with a dot circle. However, on the $CuFeO_2$ spectra, the pre-edge feature disappears as a result of the interactions with its neighbors, *i.e.*, oxygen, which provides more convenient levels (2*p*) to 1s electrons of the Cu atoms as a final state. In the delafossite structure, oxygen atoms are located at closer distances to Fe than Cu.[22] The closer distances cause an overlap between Fe-O outer shell electrons, while the Cu atoms interact with the O atoms weakly. The weak influence of the O atoms on the valence levels of the Cu atoms supports 1*s* electron transitions to the 4*p* levels, which obeys the dipole selection rules. With the increase in regular transitions, the pre-edge structure disappears.[2,4] The EXAFS part with spectral fluctuation lies beyond the absorption edge spectra as a result of photoelectron wavefunctions' interference with the incident X-rays. The data for the EXAFS analysis were derived from the measured XAFS spectra using ATHENA and ARTEMIS software.[18]

In Figure 8, the extracted chi (χ) signal of regular metal Cu foil is given as a guide reference for further scattering analysis. In the figure, Cu metal has smooth scattering signals, highlighting the uniform crystal geometry in the sample. In such a uniform material, excited photoelectrons can travel in a stable interstitial potential and scatter from the neighboring Cu atoms around 5 to 10 k values. The scattering intensities correspond to the energy of the scattering from the outer shell electrons of the neighboring Cu atoms with a degree of k^2. The k^2 value helps researchers differentiate the signals of the light and heavy atoms from each other. Heavy atoms scattering intensity have a higher increase than light atoms with a change in k value. As $k \approx 1/\lambda$, the mean free paths of the photoelectrons can be estimated from the k values. In the figure, the scattering intensity is low both at the highest and lowest k values, while the strongest intensity values are observed at the

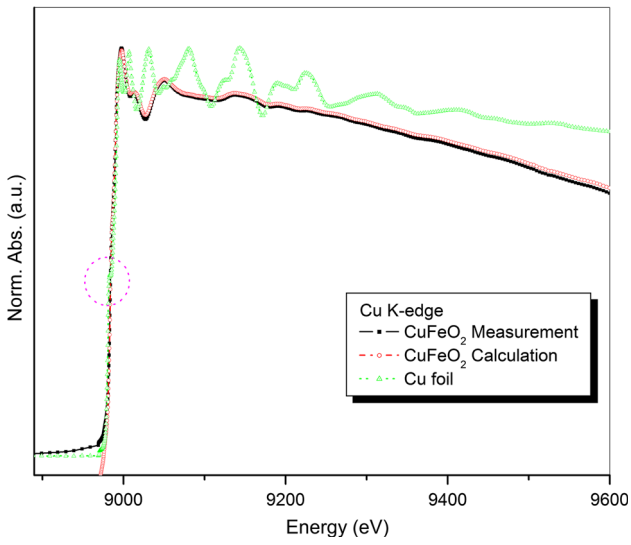

Fig. 7—Comparison of the metal copper K-edge XAFS spectra with the measured and calculated Cu K-edge spectra of the sample for $x = 0.0$. On the spectra, the weak pre-edge structure is highlighted with the red circle.

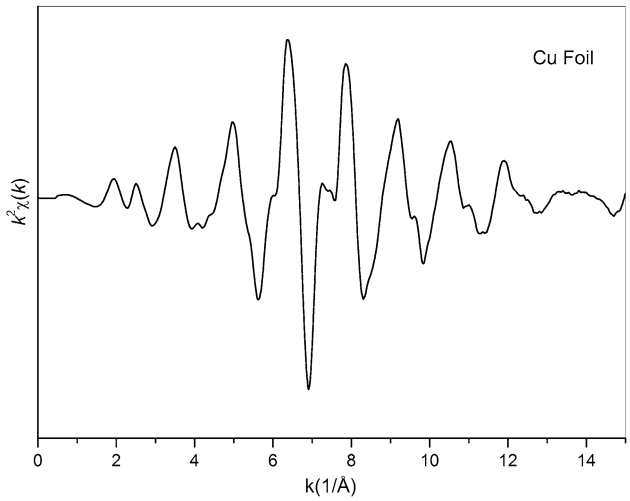

Fig. 8—EXAFS scattering intensity of Cu foil.

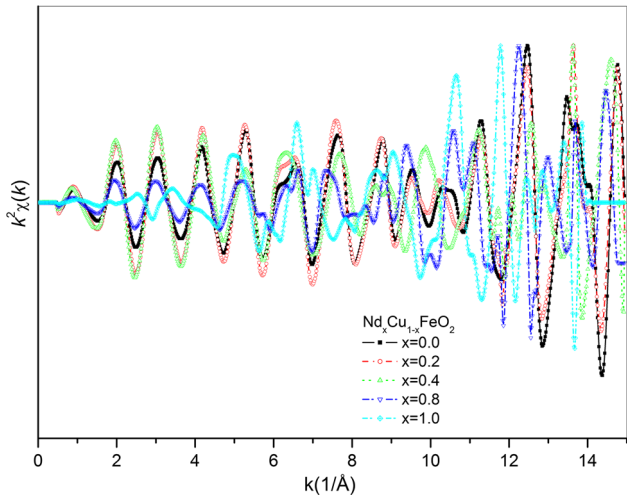

Fig. 9—EXAFS scattering intensity comparison for samples $x = 0.0$, 0.4, and 1.0.

intermediate k values (~2-Å maximum). This spectral feature implies a low-energy decay while traveling from the source atom to the neighboring Cu atoms due to the homogeneous interstitial potentials that reduce its kinetic energy slightly. Besides, the photoelectron mainly loses its energy during the single scattering and double scattering interactions.

In Figure 9, the EXAFS scattering intensity comparison of the $Nd_xCu_{1-x}FeO_2$ samples is given. The scattering intensities of the samples have noisy structure reflecting the polycrystalline formations in the samples. All of the samples have high agreement in scattering intensities at high k values, implying short mean free paths of the photoelectrons. High scattering intensities at high k values highlight the asymmetries in atomic coordinates due to polycrystalline structure, where heavy Nd atoms also presented. The sample for $x = 0.2$ has a polycrystalline structure but high symmetries in the geometries of the crystal formations that yield more symmetric scattering intensities. The noisy structures of the samples for $x = 0.4$ and 0.8 are due to the lower crystal geometries. Besides, heavy Nd and light O atoms are located in a short distance and cause multiple scatterings with high intensities, *i.e.*, short mean free path. Especially, irregular scattering intensities at high k values and high decay at low k values are a result of the heavy Nd atoms in the samples. Nd atoms are large in diameter and attract light O atoms to closer distances between the Nd-Fe interstitial region. Such an atomic diversity in the sample causes shorter path lengths of photoelectrons due to rapid energy loss because of frequent scattering from different types of atoms in a denser crystal. The photoelectrons are scattered by the outershell electrons of the neighboring atoms, so the Fourier transform of the EXAFS signals can yield the atomic locations as radial distribution function (RDF) data. The RDF is related to the one-dimensional localization of the neighboring atoms surrounding the source atom. By the EXAFS fits, one can define the exact atomic to the source atom.

The fits for the measured EXAFS spectra were performed with the generated paths from the FEFF 8.2 code calculations. In Figure 10, RDF spectra of the sample for $x = 0.0$ (80 pct $CuFeO_2$ and 20 pct α-Fe_2O_3) are given, with the RDF result of Cu foil in comparison. The multipeak structure of the $x = 0.0$ sample presents a clear image of the more complicated crystal formation in the sample than metal Cu. Besides, in different geometries, atoms can be located with slightly different distances or angles and their signals may overlap. In $CuFeO_2$ crystal, light oxygen and iron atoms are located between the Cu blocks and give multiple peaks in the short range of atomic distances. According to the RDF analysis, the distance between the source Cu atom and the closest Cu atom (*i.e.*, Cu-Cu distance) in the metal Cu sample was determined as 2.553 Å. However, in the sample for $x = 0.0$ ($CuFeO_2$), Cu-Cu distance was estimated as 3.022 Å, which means Cu atoms in metal Cu are located at closer distances. In the sample, the closest atomic distances for the other atom types were estimated as 1.644 Å for Cu-O and 3.023 Å for Cu-Fe distances.

The parent oxide $CuFeO_2$ was reported as AFM ordered at $T_N = 11$ K (−262 °C).[2] The main question for such a material can be, "What is the influence of Nd substitution on $CuFeO_2$'s magnetic properties?" For this purpose, magnetic study for $Nd_xCu_{1-x}FeO_2$ samples was also performed by the X-ray magnetic circular dichroism (XMCD) technique at room temperature without an applied external magnetic field at beamline I1011. However, no dichroic signals were collected for the samples excluding $NdFeO_3$ ($x = 1.0$). The $NdFeO_3$ sample was the only one determined to have weak AFM ordering at room temperature.

III. CONCLUSIONS

In this study, the influence of a rare earth with low electronic occupancy in the *4f* shells, neodymium, was tested to probe the *f*-electrons' behaviors in a crystal with frusturated geometry *via* electronic and crystal structure study. For this purpose, heavy fermion neodymium substitution in Cu coordinates of the $CuFeO_2$ samples on their crystal, electronic, and magnetic properties *via* the general formula $Nd_xCu_{1-x}FeO_2$ were investigated. The crystal structure analysis results revealed polycrystalline formations in the sample. Additionally, an increase in the crystalline sizes was determined coherently changing with the substituted heavy fermion Nd. Also, increasing Nd amounts were determined to cause a disturbance in the Cu-Fe planes and crystal structure formations with low symmetry.

To investigate the background information that emerges from such crystal properties, the XAFS technique was used. Prominent changes in crystal structures due to the substituted Nd atoms and phase transitions in the crystal structure were detected. In all stages of the substitutions, Nd atoms were determined to govern the entire phenomenon with their narrow 4*f* levels.

As the parent oxide $CuFeO_2$ is antiferromagnetically ordered at low temperatures [$T_N = 11$ K (−262 °C)], magnetic properties of the samples were tested at room

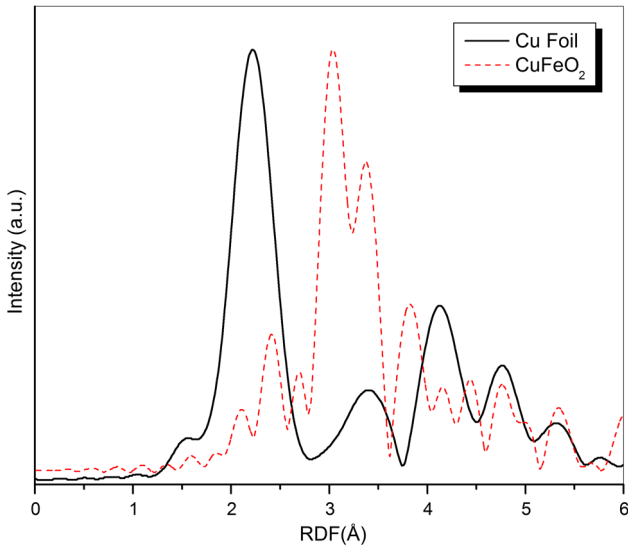

Fig. 10—Comparison of the RDF of Cu foil with the sample for $x = 0.0$.

temperature by the XMCD technique. As a result of the study, except the sample for $x = 1.0$, no dichroism was observed. In other words, most of the samples were determined to show paramagnetic behaviors at room temperature. However, only sample $NdFeO_3$ ($x = 1.0$) was determined to show weak antiferromagnetic ordering at room temperature.

ACKNOWLEDGMENTS

The author thanks Dr. Gunnar Ohrwall, MAX-lab. Beamline I1011 (Lund, Sweden). The author also thanks Dr. B. Nirawat Thammajak, Dr. Wantana Klyusubun, and the staff of BL8 from SLRI (Siam Photon) of Thailand, both for their technical support and great hospitality. This study was supported financially by the "2015-AP4-1153" project of Mersin University (Mersin, Turkiye). Additionally, the research leading to these results has received funding from the European Community's Seventh Framework Program (FP7/2007-2013) CALIPSO under Grant Agreement No. 312284.

REFERENCES

1. P.S. Miedema and M.F. De Frank: GrootJ. *Electron Spectrosc Relat. Phenom.*, 2013, vol. 187, pp. 32–48.
2. O.M. Ozkendir: *J. Electron. Mater.*, 2013, vol. 42 (6), pp. 1055–62.
3. K. Mori, M. Hachisu, T. Yamazaki, and Y. Ichiyanagi: *J. Appl. Phys.*, 2015, vol. 117, p. 17C756, DOI:10.1063/1.4919328.
4. O.M. Ozkendir: *J. Optoelectron. Adv. Mater. Rapid Commun.*, 2009, vol. 3, pp. 586–91.
5. H. Takahashi, Y. Motegi, R. Tsuchigane, and M. Hasegawa: *J. Magn. Magn. Mater.*, 2004, vol. 217, pp. 272–76.
6. C. Ruihua, C.N. Borca, P.A. Dowbena, S. Stadler, and Y.U. Idzerda: *Appl. Phys. Lett.*, 2001, vol. 78 (4), pp. 521–23.
7. E. Dagotto: *Science*, 2005, vol. 309 (5732), pp. 257–62.
8. H.S. Nabi and R. Pentcheva: *Phys. Rev. B*, 2011, vol. 83, pp. 214424–5.
9. E.A. Moore: *Phys. Rev. B*, 2007, vol. 76, p. 195107.
10. B. Klobes, M. Herlitschke, K.Z. Rushchanskii, H.C. Wille, T.T.A. Lummen, P.H.M. van Loosdrecht, A.A. Nugroho, and R.P. Hermann: *Phys. Rev. B*, 2015, vol. 92, pp. 014304–9.
11. A. Monshi, M.R. Foroughi, and M.R. Monshi: *World J. Nano Sci. Eng.*, 2012, vol. 2, pp. 154–60.
12. A. Gholizadeh: *J. Adv. Mater. Process.*, 2015, vol. 3 (3), pp. 71–83.
13. S.K. Chawla, S.S. Meena, P. Kaur, R.K. Mudsainiyan, and S.M. Yusuf: *J. Magn. Magn. Mater.*, 2015, vol. 378, pp. 84–91.
14. L. Lutterotti, M. Bortolotti, G. Ischia, I. Lonardelli, and H.-R. Wenk: *Z. Kristallogr. Suppl.*, 2007, vol. 26, pp. 125–30.
15. I.A. Kowalik, G. Öhrwall, B.N. Jensen, R. Sankari, E. Wallen, U. Johansson, O. Karis, and D. Arvanitis: *J. Phys.*, 2010, vol. 211, p. 012030, DOI:10.1088/1742-6596/211/1/012030.
16. J. Stöhr: in *NEXAFS spectroscopy*, H.K.V. Lotsch, ed., Springer, Heidelberg, 2003.
17. A.L. Ankudinov, B. Ravel, J.J. Rehr, and S.D. Conradson: *Phys. Rev. B*, 1997, vol. 56, pp. R1712–16.
18. B. Ravel: *J. Synchrotron Rad.*, 2001, vol. 8 (2), pp. 314–16.
19. W. Klysubun *et al.*: *Nucl. Instrum. Meth. Phys. Res. A*, 2007, vol. 582, pp. 87–89.
20. Klysubun *et al.*: *AIP Conf. Proc.*, 2006, vol. 879, pp. 860–63.
21. B. Ravel and M. Newville: *J. Synchrotron Rad.*, 2005, vol. 12 (4), pp. 537–41.
22. H. Takahashi, Y. Motegi, R. Tsuchigane, and M. Hasegawa: *J. Magn. Magn. Mater.*, 2004, vol. 217, pp. 272–76.